

Baryon number fluctuations at finite temperature and density

Wei-jie Fu,^{1,2} Jan M. Pawłowski,^{2,3} Fabian Rennecke,^{2,4} and Bernd-Jochen Schaefer⁴

¹*Institute of Theoretical Physics, School of Physics & Optoelectronic Technology,
Dalian University of Technology, Dalian, 116024, P.R. China*

²*Institut für Theoretische Physik, Universität Heidelberg, Philosophenweg 16, 69120 Heidelberg, Germany*

³*ExtreMe Matter Institute EMMI, GSI, Planckstr. 1, 64291 Darmstadt, Germany*

⁴*Institut für Theoretische Physik, Justus-Liebig-Universität Gießen, Heinrich-Buff-Ring 16, 35392 Gießen, Germany*

We investigate baryon number fluctuations for finite temperature and density in two-flavor QCD. This is done within a QCD-improved low-energy effective theory in an extension of the approach put forward in [1, 2]. In the present work we aim at improving the predictive power of this approach for large temperatures and density, that is, for small collision energies. This is achieved by taking into account the full frequency dependence of the quark dispersion. This ensures the necessary Silver Blaze property of finite density QCD for the first time, which so far was only implemented approximately. Moreover, we show that Polyakov loop fluctuations have a sizeable impact at large temperatures and density. The results for the kurtosis of baryon number fluctuations are compared to previous effective theory results, lattice results and recent experimental data from STAR.

PACS numbers: 11.30.Rd, 11.10.Wx, 05.10.Cc, 12.38.Mh

I. INTRODUCTION

The past years have seen rapid progress of our understanding of heavy-ion collision physics and QCD in extreme conditions. This progress has been achieved by both experimental measurements at the Relativistic Heavy-Ion Collider (RHIC) and the Large Hadron Collider (LHC), as well as theoretical calculations made in various ab initio and effective theory approaches. One of the remaining key challenges is to get hold of the existence and location of the critical end point (CEP) in the QCD phase diagram [3]. Experimentally, the search of the CEP is under way in the Beam Energy Scan (BES) program at RHIC [4–6], as well as future searches at the FAIR and NICA facilities, and the evaluation of current results at low collision energies at HADES, spanning a wide collision energy or density regime, see [7]. On the theoretical side, first principle lattice computations are hampered by the notorious sign problem at finite chemical potential [8]. First principle functional continuum computations are hampered by the task of systematically taking into account the relevant degrees of freedom [9]. This calls for refined effective theory investigations that are embedded in QCD such, that they allow for a systematic improvement towards full QCD. This approach is taken in the current work, extending the recent works [1, 2].

Correlations of conserved charges provides good experimental signatures of the CEP: as the transition at the CEP is of second order, a singularity is expected in thermodynamic quantities. However, since the QGP produced in heavy-ion collisions is finite both spatially and temporally, such singularities cannot be observed in Nature. Nonetheless, fluctuations in event-by-event multiplicity distributions of conserved quantities such as variances and moments of these distributions become more sensitive around the CEP since their criticality are proportional to powers of the correlation length [10–

12]. This intuitive physical picture is the foundation for present and future experimental searches for the critical end point. In the present work, we investigate baryon number fluctuations which are described by the generalised susceptibilities and are given by derivatives of the pressure p with respect to the baryon chemical potential $\mu_B = 3\mu$. Thus, the accurate description of baryon number fluctuations requires a thorough understanding of the chemical potential dependence of the equation of state of QCD. But this is still a formidable problem in theoretical QCD investigations and far from being solved.

Furthermore, since the created quark-gluon plasma is of finite spatial extent and cools down rapidly, the system evolves out of equilibrium in the vicinity of the CEP. Due to the critical slowing down phenomenon long equilibration times are expected and the correlation length cannot grow as fast as its equilibrium counterpart in the expanding plasma [13]. As a consequence, the generalised susceptibilities measured in the experiment could differ in both magnitude and sign from the equilibrium prediction in the critical region [14, 15].

Nonetheless, understanding the chemical potential dependence of the equation of state in equilibrium is a crucial building block for a deeper comprehension of the signatures of the CEP in heavy-ion collisions. Recently, some of us have investigated the QCD thermodynamics, the skewness and the kurtosis of the baryon number distributions within QCD-improved low-energy effective models [1, 2], for related work see also [16–27]. In these computations quantum, thermal, and density fluctuations are embedded with the functional renormalisation group (FRG) approach to QCD, see e.g. [9, 28–33] and references therein. In the present work, we significantly improve on these previous studies.

The chemical potential dependence of the equation of state of QCD is intimately linked to a peculiar feature of finite density QCD known as the Silver Blaze property [34]. It states that at vanishing temperature observables

are independent of the chemical potential below a critical one. A proper description of QCD at finite chemical potential has to respect this property. In the context of the functional renormalisation group, it was shown that the Silver Blaze property is directly linked to the frequency dependence of correlation functions that involve particles with non-vanishing baryon number [1, 35]. We have generalised the previous works and have implemented for the first time frequency dependent quark correlation functions to the equation of state. This fully guarantees the Silver Blaze property in such a fluctuation analysis. As we shall see these modifications have a significant effect on both the magnitude and the sign of the kurtosis of baryon number fluctuations at finite density.

Another related crucial issue in this respect is how the gluon fluctuations and confinement affect the baryon number fluctuations. In the low-energy sector of QCD, gluon effects are implemented in a non-vanishing gluon background field whose thermodynamics is encoded in a Polyakov loop potential. It has been argued in [1] that the baryon number susceptibilities are rather sensitive to Polyakov loop fluctuations. Hence, we include a phenomenological Polyakov loop potential that captures the effect of Polyakov loop fluctuations [36]. Such a potential incorporates the back-reaction of the gluon effects on the matter sector of QCD. This significantly influences the baryon number fluctuations at temperatures above T_c .

The paper is organised as follows: In Sec. II we briefly introduce the approach of QCD-improved low-energy effective theories within the FRG framework. In Sec. III the flow equations in the presence of a frequency dependent quark anomalous dimension are discussed and some implications are discussed. Numerical results, their discussion and comparison with lattice and experimental data are provided in Sec. IV. A summary with our conclusions can be found in Sec. V and technical details on the used threshold functions are collected in the appendix.

II. FRG FOR QCD AND THE LOW ENERGY EFFECTIVE THEORY

In this work we improve the previous studies [1, 2] on baryon number fluctuations within a low-energy effective theory in two aspects: Firstly, we extend the approximation to the off-shell fluctuation physics used in the previous works. This is important for both quantitative precision as well as the systematic error control in the present approach. This leads us to an improved effective potential, where the fluctuation-induced and frequency-dependent corrections to the quark dispersion are taken into account. These improvements are important for the proper description of baryon number fluctuations in particular at finite chemical potential due to the intimate relation between the frequency dependence of correlation functions and the chemical potential dependence of the theory. This will be elaborated in detail in the following section. Secondly, the improved fluctuation analy-

sis is extended to the glue sector. Here we incorporate a Polyakov loop potential which captures the Polyakov loop fluctuations [36]. Such a potential takes into account the impact of off-shell fluctuations beyond the level of expectation values of the Polyakov loop variable and the thermodynamics. Such an extension has been argued to be important in [1] for the evaluation of the baryon number fluctuations.

We begin with the discussion of the effective model. It is based on the description of low-energy QCD for two flavors put forward in [1, 30, 37]. Here, we give a brief summary and refer the interested reader to the literature for details. In order to capture the relevant hadronic degrees of freedom at small and intermediate densities, we include the pion and the sigma mesons as the dominant low-energy degrees of freedom. They are coupled to quarks via a Yukawa interaction term with a running coupling h_k . The purely mesonic interactions are stored in the effective potential $V_k(\rho)$ with $\rho = (\vec{\pi}^2 + \sigma^2)/2$. Fluctuation-induced corrections to the classical quark and meson dispersion relations are taken into account by the corresponding quark and meson wave function renormalisations $Z_{q,k}$ and $Z_{\phi,k}$. Due to the dynamical generation of the gluon mass gap, the gluon sector of QCD decouples at low energies $\Lambda \lesssim 1$ GeV and the informations of the deconfinement transition are encoded in a non-vanishing gluon background field for energies $k < \Lambda$. We therefore introduce a non-vanishing temporal gluon background field A_0 which couples to the quarks as well as to a corresponding effective potential $V_{\text{glue}}(L, \bar{L})$. The potential is formulated in terms of the expectation value of the traced Polyakov loop L and its adjoint \bar{L} . They are given by

$$L(\vec{x}) = \frac{1}{N_c} \langle \text{tr } \mathcal{P}(\vec{x}) \rangle, \quad \bar{L}(\vec{x}) = \frac{1}{N_c} \langle \text{tr } \mathcal{P}^\dagger(\vec{x}) \rangle, \quad (1)$$

with

$$\mathcal{P}(\vec{x}) = \mathcal{P} \exp \left(ig \int_0^\beta d\tau A_0(\vec{x}, \tau) \right). \quad (2)$$

We postpone the introduction and discussion of the Polyakov loop potential $V_{\text{glue}}(L, \bar{L})$ to the next section.

Such a construction results in a Polyakov-quark-meson (PQM) model [38] and the corresponding effective action reads

$$\begin{aligned} \Gamma_k = \int_x \Big\{ & Z_{q,k} \bar{q} [\gamma_\mu \partial_\mu - \gamma_0 (\mu + ig A_0)] q + V_{\text{glue}}(L, \bar{L}) \\ & + \frac{1}{2} Z_{\phi,k} (\partial_\mu \phi)^2 + h_k \bar{q} \left(T^0 \sigma + i \gamma_5 \vec{T} \vec{\pi} \right) q + V_k(\rho) - c\sigma \Big\}, \end{aligned} \quad (3)$$

with $\int_x = \int_0^{1/T} dx_0 \int d^3x$ and the quark chemical potential μ . The gluonic background field is constant and only its temporal component assumes a non-vanishing expectation value. The real meson field $\phi = (\sigma, \vec{\pi})$ is in the $O(4)$ -representation, and $\rho = \phi^2/2$. The $SU(N_f)$

generators \vec{T} are normalised as $\text{tr}(T^i T^j) = \frac{1}{2} \delta^{ij}$ with $T^0 = \frac{1}{\sqrt{2N_f}} \mathbb{1}_{N_f \times N_f}$. The chiral effective potential $V_k(\rho)$ is $O(4)$ invariant, and the linear term $-\sigma$ breaks chiral symmetry explicitly. Note that the matter and the gauge sector of QCD are naturally coupled to each other by considering a non-vanishing gluon background. The background field A_0 enters the chiral effective potential V_k through quark fluctuations [39]. In this way the correct temperature scaling of the gluon potential in QCD is recovered: at vanishing density and finite current quark masses, both the chiral and the deconfinement transition are smooth crossovers. This also holds for thermodynamical quantities like the pressure and trace anomaly. With such a QCD-enhanced glue potential and for $N_f = 2 + 1$ quark flavor nice agreement with recent lattice QCD results can be obtained, see [29].

All couplings in the effective action depend on the renormalisation group (RG) scale k . By following the evolution of Γ_k from the UV cutoff scale $k = \Lambda$ down to the infrared $k = 0$, quantum fluctuations are successively included in the effective action. The evolution equation for $\Gamma_k[\Phi]$, where $\Phi = (A_\mu, c, \bar{c}, q, \bar{q}, \phi, \dots)$ indicates the super field, is given by the Wetterich equation [40],

$$\partial_t \Gamma_k[\Phi] = \frac{1}{2} \text{Tr} G_{\Phi\Phi}[\Phi] \partial_t R_k^\Phi, \quad t = \ln(k/\Lambda), \quad (4)$$

with the exact field-dependent propagator

$$G_{\Phi_i \Phi_j}[\Phi] = \left(\frac{1}{\frac{\delta^2 \Gamma_k[\Phi]}{\delta \Phi^2} + R_k^\Phi} \right)_{ij}, \quad (5)$$

and a regulator R_k^Φ . Within this framework, it is by now well understood how the used effective low-energy model is embedded into full QCD. To that end we rewrite the effective action as

$$\Gamma_k[\Phi] = \Gamma_{\text{glue},k}[\Phi] + \Gamma_{\text{matt},k}[\Phi], \quad \Gamma_{\text{matt},k} = \Gamma_{q,k} + \Gamma_{\phi,k}, \quad (6)$$

where $\Gamma_{\text{glue},k}$ encodes the ghost- and gluon fluctuations and is the glue sector of the effective action. The matter sector $\Gamma_{\text{matt},k}$ is composed of $\Gamma_{q,k}[\Phi]$ arising from quark fluctuations, and $\Gamma_{\phi,k}[\Phi]$ from that of the hadronic degrees of freedom, see Fig 1. The separation between the quark and hadronic contributions is realised through the dynamical hadronisation [41–44], a very efficient parameterisation of matter fluctuations in ab initio QCD, for applications to QCD see e.g. [32, 33].

The gluon and ghost fluctuations start to decouple from the matter sector after the QCD-flow is integrated down to scales $k = \Lambda$ with $\Lambda \lesssim 1$ GeV, for more details, see e.g., [32, 33]. We are left with an effective matter theory with a glue background, which is given by Polyakov-loop-extended chiral models, such as the Polyakov–Nambu–Jona-Lasinio model [39, 45, 46] and the Polyakov–quark-meson (PQM) model [38]. For further details in this direction, we refer to recent works and reviews, e.g. [9, 32, 33, 47, 48].

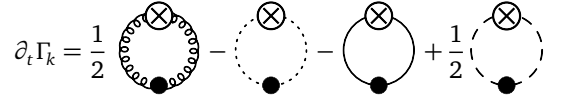


FIG. 1. Flow of the effective action. The first two diagrams are the gluon and ghost contributions. Here, they are assumed to be integrated out. The low-energy information of the gluon sector is stored in an effective Polyakov loop potential. The last two diagrams are the matter contributions to the flow, i.e. quarks and mesons in the present case. The black dots indicate that the fully dressed propagators are involved in the flow equation. The crossed circles denote the regulator insertion.

In summary, below the decoupling scale of the glue sector we are left with an effective theory that is well described with an effective action (3). Further quantum, thermal and density fluctuations are then obtained by the flow equation with the remaining dynamical degrees of freedom, the quarks and mesons. Within the present approximation this boils down to the low-energy QCD-flows used in [33] in the vacuum. For the computation of baryon number fluctuations derivatives of the pressure with respect to the quark chemical potential are needed. The pressure is extracted from the scale dependent effective action Γ_k , (3), in the infrared via the thermodynamic potential

$$\Omega[\Phi; T, \mu] = V_{\text{glue}}(L, \bar{L}) + V_{k=0}(\rho) - c\sigma. \quad (7)$$

Eq. (7) simply constitutes the effective action $\Gamma_{k=0}$ at vanishing cutoff scale k , evaluated on constant backgrounds L, \bar{L}, σ . Finally the backgrounds are chosen such that they solve the equations of motion (EoM): Φ_{EoM} . The rest of the fields vanish on the EoMs, so they are taken to be zero straightaway. Then the normalised pressure reads

$$p(T, \mu) = -\Omega[\Phi_{\text{EoM}}; T, \mu] + \Omega[\Phi_{\text{EoM}}; 0, 0]. \quad (8)$$

Hence, by solving the flow equation (4) for the effective action (3), we extract the pressure and obtain the baryon number fluctuations from appropriate μ -derivatives. The latter are defined by the generalised susceptibilities

$$\chi_n^B = \frac{\partial^n}{\partial(\mu_B/T)^n} \frac{p}{T^4}, \quad (9)$$

which are given as n^{th} -derivatives of the pressure p with respect to the baryon chemical potential μ_B related to the quark chemical potential by $\mu = \mu_B/3$.

Cumulants of baryon multiplicity distributions, which can be measured experimentally, are closely related to the generalised susceptibilities χ_n^B , such as the variance $\sigma^2 = VT^3 \chi_2^B$ or the kurtosis $\kappa = \chi_4^B / (\chi_2^B \sigma^2)$. All generalised susceptibilities depend on the volume V of the system which drops out by considering ratios like the kurtosis of the susceptibilities.

A. Fluctuations and the Polyakov Loop Potential

It follows from the discussion of the last chapter that the glue part of the potential cannot be obtained within the present effective theory approach, which only considers quark and meson fluctuations below the glue decoupling scale. Moreover, the quarks couples to the mean temporal gauge field, $\langle A_0 \rangle$, rather than the mean Polyakov loop L defined in (1). For a related detailed discussion and a computation and comparison of both observables see [49].

In the present work we shall ignore this issue, and instead resort to utilising pure glue lattice data. In absence of a lattice computations of the Polyakov loop potential $V(L, \bar{L})$ in $SU(3)$, Yang-Mills lattice data on correlation functions are used. This includes the thermal pressure p , the Polyakov loop expectation value L , and the fluctuations, e.g. $\langle \text{tr } \mathcal{P}(\vec{x}) \text{tr } \mathcal{P}(\vec{y}) \rangle$ with \mathcal{P} defined in (2). These observables determine the minimum of the potential (L), the value of the potential at the minimum (p), as well as all second derivatives $\partial_{L, \bar{L}}^2 V$ w.r.t. L, \bar{L} at the minimum. Finally, the temperature scales in the pure glue potentials have to be adapted to full dynamical QCD as has been put forward in [28, 29]. In the present context this has been discussed in [1]. In summary it amounts to the rescaling of the reduced temperature $t = T/T_0$ in the Yang-Mills potential by a factor 0.57. Here T_0 is the Yang-Mills critical temperature. In the present set-up the absolute temperature scale T_0 is fixed by the requirement of equivalent confinement-deconfinement pseudo-critical and chiral critical temperatures in the chiral limit as predicted in [50].

It is left to choose the specific parameterisation of the pure glue potential. There are various possibilities to model such a Polyakov loop potential. Most commonly used potentials are either of polynomial [45] or logarithmic form [51]. These standard potentials only utilise the temperature dependence of the pressure p and the expectation value L , for a comparison see e.g. [52]. More recently, the quadratic fluctuations of the Polyakov loop have also been computed in [36]. A polynomial potential with an additional logarithmic term including the Haar measure M_H of the $SU(3)$ gauge group describes the lattice results for the Polyakov loop fluctuations remarkably well. It reads

$$V_{\text{glue}}(L, \bar{L}) = -\frac{a(T)}{2} \bar{L}L + b(T) \ln M_H(L, \bar{L}) + \frac{c(T)}{2} (L^3 + \bar{L}^3) + d(T) (\bar{L}L)^2, \quad (10)$$

with the Haar measure as a function of the Polyakov loop and its conjugate,

$$M_H(L, \bar{L}) = 1 - 6\bar{L}L + 4(L^3 + \bar{L}^3) - 3(\bar{L}L)^2. \quad (11)$$

The temperature-dependent coefficients in (10) can be

	1	2	3	4	5
a_i	-44.14	151.4	-90.0677	2.77173	3.56403
b_i	-0.32665	-82.9823	3.0	5.85559	
c_i	-50.7961	114.038	-89.4596	3.08718	6.72812
d_i	27.0885	-56.0859	71.2225	2.9715	6.61433

TABLE I. Coefficients of the Polyakov loop potential parameterisation Eqs. (12) and (13).

expressed by the following parameterisation

$$x(T) = \frac{x_1 + x_2/t + x_3/t^2}{1 + x_4/t + x_5/t^2}, \quad (12)$$

for $x \in \{a, c, d\}$ and $t = T/T_0$ whereas $b(T)$ reads

$$b(T) = b_1 t^{-b_4} (1 - e^{b_2/t^{b_3}}). \quad (13)$$

For the deconfinement temperature we use $T_0 = 250$ MeV. The coefficients are collected in Tab. I. Note in this context that in [1] it was shown analytically that the higher moments of the baryon number distribution crucially depend on the Polyakov loop propagators. Furthermore, the Polyakov loop susceptibilities computed in [36] are proportional to the connected two-point functions of the loops. They are therefore directly related to their propagators. Thus, since this parameterisation is optimised for the description of the Polyakov loop propagators, which in turn are the crucial contributions of the pure glue sector of QCD to the baryon number fluctuations, the potential in Eq. (10) is the most natural choice for the present purpose.

This potential reduces to the polynomial potential for $b(T) = 0$, i.e. when the logarithmic term is dropped. While both parameterisations give the same results for $T < T_c$, the results for the Polyakov loop susceptibilities deviate largely for $T > T_c$. Hence, based on the discussion above, we expect improvements of the previous results in Ref. [1, 2] on the baryon number fluctuations for $T > T_c$. We demonstrate this explicitly in Sec. IV.

III. CORRELATION FUNCTIONS AT FINITE DENSITY AND SILVER BLAZE

A. Silver Blaze Property and the Frequency Dependence

At vanishing temperature the quark chemical potential has to exceed a critical value μ_c before the system can reach a finite density. This is known as the Silver Blaze property [34]. In the context of the FRG, the consequences of the Silver Blaze property have been discussed first in [1, 35] and we refer to this work for a more thorough discussion.

As a consequence, all QCD observables at $T = 0$ are independent of the chemical potential for $\mu \leq \mu_c$. The quark critical chemical potential $3\mu_c = M_N - \epsilon_b$ is close to

the pole mass of the lowest lying state with non-vanishing baryon number, i.e., the nucleon mass M_N . The subtraction ϵ_b accounts for the binding energy of nuclear matter. In the present work we drop the small binding energy ϵ_b and also identify $M_N = 3M_q$. Formally, this property entails for $\mu \leq \mu_c$ that the μ -dependence of the correlation functions is given by a simple shift of the frequency arguments. For the present discussion it is convenient to decompose the scale-dependent 1PI finite density correlation functions

$$\Gamma_{\Phi_1 \dots \Phi_n, k}^{(n)}(p_1, \dots, p_n; \mu) = \frac{\delta^n \Gamma_k}{\delta \Phi_1(p_1) \dots \delta \Phi_n(p_n)}, \quad (14)$$

into the vertex function and the momentum conservation,

$$\begin{aligned} & \Gamma_{\Phi_1 \dots \Phi_n, k}^{(n)}(p_1, \dots, p_n; \mu) \\ &= \tilde{\Gamma}_{\Phi_1 \dots \Phi_n, k}^{(n)}(p_1, \dots, p_{n-1}; \mu) (2\pi)^4 \delta(p_1 + \dots + p_n). \end{aligned} \quad (15)$$

The δ -function involves that we count all momenta as incoming. Then the Silver Blaze property is entailed in simple equations for the vertex functions (15) for $\mu < \mu_c$,

$$\tilde{\Gamma}_{\Phi_1 \dots \Phi_n, k}^{(n)}(p_1, \dots, p_{n-1}; \mu) = \tilde{\Gamma}_{\Phi_1 \dots \Phi_n, k}^{(n)}(\tilde{p}_1, \dots, \tilde{p}_{n-1}; 0), \quad (16)$$

with the shifted Euclidean four-momenta

$$\tilde{p}_j = (p_{0j} + i\alpha_j \mu, \vec{p}_j), \quad j = 1, \dots, n. \quad (17)$$

The baryon number of the corresponding fields Φ_j is given by $\alpha_j/3$. As the baryon number of all $\Gamma_k^{(n)}$ vanishes we have $\tilde{p}_1 + \dots + \tilde{p}_n = p_1 + \dots + p_n$, the sum of the \tilde{p}_i is real. Hence the property (16) formally extends to the full correlation functions with $\delta(\tilde{p}_1 + \dots + \tilde{p}_n)$ being well-defined.

The intimate relation between the Silver Blaze property and the frequency dependence of n -point functions is manifest in Eq. (16). This has important consequences for consistent approximation schemes: if the frequency dependence of correlation functions is not taken into account properly, the Silver Blaze property is violated. This applies to all n -point functions involving legs with nonzero baryon number.

In the present work, these are the running Yukawa coupling h_k and the quark anomalous dimension $\eta_{q,k} = -\frac{\partial_t Z_{q,k}}{Z_{q,k}}$. For example, in the spirit of (16) the Yukawa coupling reads for $\mu \leq \mu_c$

$$\tilde{\Gamma}_{q\bar{q}\phi, k}^{(3)}(p_1, p_2; \mu) \propto h_k(\tilde{p}_1, \tilde{p}_2), \quad (18)$$

with \tilde{p}_i as in (17) with $\alpha_1 = -\alpha_2 = 1$ and $\alpha_3 = 0$, and we have dropped all terms with other tensor structures of the vertex. This entails that $\tilde{p}_1 + \tilde{p}_2 = p_1 + p_2$ and $\tilde{p}_3 = p_3$. Note again that all momenta p_i are incoming momenta. The μ -dependent frequencies for quark and anti-quark read $\tilde{p}_{01} = p_{01} + i\mu$, $\tilde{p}_{02} = p_{02} - i\mu$. Similarly it follows for the quark anomalous dimension

$$\partial_t \tilde{\Gamma}_{q\bar{q}, k}^{(2)}(p; \mu) \propto \eta_{q,k}(\tilde{p}) \gamma_\mu \tilde{p}_\mu, \quad (19)$$

using the momentum conservation $\tilde{p}_1 = -\tilde{p}_2$. As in (18) we have dropped terms with further tensor structures in (19), here it is only the scalar one proportional to the quark mass and its flow. We conclude that for $\mu < \mu_c$ we have

$$\partial_\mu|_{\tilde{p}_i} h_k(\tilde{p}_1, \tilde{p}_2) = \partial_\mu|_{\tilde{p}} \eta_{q,k}(\tilde{p}) = 0. \quad (20)$$

Hence, neither the wave function renormalisation Z_q nor the Yukawa coupling receive a genuine μ -dependence. At vanishing temperature the density or chemical potential contributions to the flow equation are proportional to the step function $\Theta(\mu - E_{q,k})$, with the quasi-particle energies for the quarks $E_{q,k} = \sqrt{k^2 + M_{q,k}^2}$. For $\mu > \mu_c$ the density contributions are non-vanishing. Furthermore, the explicit μ -dependence cannot be accounted anymore for by a shift of the momentum arguments as in Eq. (16). This results in manifestly μ -dependent correlation functions.

Of course, for $T > 0$ the step function becomes a Fermi distribution function $n_F(\tilde{m}_{q,k}^2; T, \mu)$ defined in (A7). So strictly speaking QCD has no Silver Blaze property at finite temperature. It is nonetheless crucial for the correct μ -dependence of the theory to carefully evaluate the frequency dependence of finite temperature correlation functions. For physical observables, they enter through the corresponding loop diagrams, for example through the quark loop contribution to the effective potential. In this case, their frequency dependence has to be taken into account in the loop integration. This is discussed in detail in the next section. If one is interested in the n -point functions themselves, they should be evaluated at complex frequencies $p_{0j} - i\alpha_j \mu$ in order to retain the Silver Blaze property. This can be seen explicitly e.g. in (A5). Such an evaluation point guarantees that the correlation functions are defined at μ -independent points in momentum space. We want to emphasise that, in any case, frequency-independent approximation schemes will always lead to a certain Silver Blaze violation and a corresponding inaccurate dependence on the chemical potential.

Moreover, the complex frequency argument $p_0 + i\mu$ in (A5) renders h_k and $\eta_{q,k}$ complex-valued. Through the corresponding loop diagrams these quantities appear in thermodynamic observables or particle masses which, in turn, have to be real-valued. In the next section we demonstrate explicitly at the example of $\eta_{q,k}$ that in due consideration of the frequency dependence real-valued quantities are finally obtained.

B. Improved Effective Potential

Since higher moments of the baryon number distribution are defined via chemical potential derivatives of the effective potential, see Eq. (9), it is of major importance that the μ -dependence of the effective potential is

resolved properly. As mentioned above, this is intrinsically tied to the Silver Blaze property of QCD and the frequency dependence of the quark-involved correlation functions. More specifically, the correlation functions that drive the flow of the effective potential are the ones for the Yukawa coupling h_k and for the quark anomalous dimension $\eta_{q,k}$. The former quantity enters the flow of the effective potential through the quark mass $m_{q,k} = h_k \sigma_0/2$ and the latter through the scale derivative of the quark regulator, $\partial_t R_k^q(\vec{p}) \propto \vec{\gamma} \vec{p} (\partial_t - \eta_{q,k}) r_F(\vec{p})$, with the fermionic regulator shape function r_F . Consequently, it is the quark loop contribution to the potential flow where the frequency dependence needs to be taken into account thoroughly.

Furthermore, only the spatial three-momenta and not the frequencies are regularised. The ensuing non-locality in frequency requires the full frequency dependence of correlation functions for quantitative precision. In turn, we use $\vec{p} = 0$, which has been shown in [31] to be a good approximation.

Now we apply this reasoning to the quark correlation functions in the present approximation (3), $Z_{q,k}, h_k$. Note that the flow of both these couplings can be deduced from that of the quark-anti-quark two-point function, see [1, 30]. In the present approximation this two-point function reads at vanishing pion fields, $\vec{\pi} = 0$,

$$\tilde{\Gamma}_{q\bar{q},k}^{(2)}(p) = Z_{q,k}(p) \left(\not{p} + \frac{\bar{h}_k(p)\bar{\sigma}}{2} \right), \quad (21)$$

where $\tilde{\Gamma}_{q\bar{q},k}^{(2)}(p)$ is the two point function without the momentum-conserving δ -function, see (15). We have also introduced the normalised couplings

$$\bar{h}_k(p) = \frac{h_k(p, -p)}{Z_{q,k}(p)Z_{\phi,k}^{1/2}(0)}, \quad \bar{\sigma} = Z_{\phi,k}^{1/2}(0)\sigma, \quad (22)$$

in the spirit of the present derivative expansion of the mesonic sector. Now we retain the frequency dependence of the dispersion via a quark wave function renormalisation $Z_{q,k}(p_0)$. As discussed before, its spatial momentum dependence is well-captured by the k -dependence of Z_k , for a detailed study see [31]. There it has been shown that $Z_k(p) \approx Z_k(0)$ is a quantitative approximation for the regularised momentum directions. The Yukawa term $\bar{h}_k(p)\bar{\sigma}/2$ relates to the momentum-dependent renormalisation group invariant (but cutoff-dependent) mass function $M_{q,k}(p)$ of the quark. This quantity has been studied with the FRG in [32] in vacuum QCD. From [32, 33] we deduce that its momentum-dependence for the current cutoff scales of $k \lesssim 700$ MeV is negligible, and we resort to a momentum-independent approximation. Naively this suggests $p = 0$. However, in order to guarantee the Silver Blaze property we evaluate the flow of $\bar{h}_k(p)$ at $\text{Im } p_0 = -i\mu$ and $\vec{p} = 0$. The real part of p_0 is adjusted for capturing the correct thermal decay, the details are given below. This ensures that the dependence on \vec{p} is not confused with a genuine μ -dependence of \bar{h}_k , see the discussion in the previous chapter and [1].

This leaves us with the task of calculating the frequency-dependent quark anomalous dimension $\eta_{q,k}(p_0)$. It is obtained from the flow of the quark two-point function (21) by the following projection prescription

$$\eta_{q,k}(p) = \frac{1}{Z_{q,k}(p)} \frac{1}{4N_c N_f} \frac{\partial^2}{\partial |\vec{p}|^2} \text{Tr} \left(i\vec{\gamma} \cdot \vec{p} \partial_t \tilde{\Gamma}_{q\bar{q},k}^{(2)}(p) \right). \quad (23)$$

By only keeping the frequency dependence and ignoring the spatial momenta by setting $\vec{p} = 0$, we arrive at

$$\begin{aligned} \eta_{q,k}(p_0) &= \frac{1}{24\pi^2 N_f} (4 - \eta_{\phi,k}) \bar{h}_k^2 \\ &\times \left\{ (N_f^2 - 1) \mathcal{FB}_{(1,2)}(\bar{m}_{q,k}^2, \bar{m}_{\pi,k}^2; p_0) \right. \\ &\left. + \mathcal{FB}_{(1,2)}(\bar{m}_{q,k}^2, \bar{m}_{\sigma,k}^2; p_0) \right\}. \end{aligned} \quad (24)$$

The threshold function $\mathcal{FB}_{(1,2)}$ is defined in App. A. Eq. (24) depends on the meson anomalous dimension $\eta_{\phi,k}(q)$. It has been evaluated at vanishing spatial momenta and frequency, $q = 0$. In this approximation it has been derived in [30] and reads,

$$\begin{aligned} \eta_{\phi,k} &= \frac{1}{6\pi^2} \left\{ \frac{4}{\bar{k}^2} \bar{\kappa}_k (\bar{V}_k''(\bar{\kappa}_k))^2 \mathcal{BB}_{(2,2)}(\bar{m}_{\pi,k}^2, \bar{m}_{\sigma,k}^2) \right. \\ &\quad + N_c \bar{h}_k(\bar{\kappa}_k)^2 [(2\eta_{q,k} - 3) \mathcal{F}_{(2)}(\bar{m}_{q,k}^2) \\ &\quad \left. - 4(\eta_{q,k} - 2) \mathcal{F}_{(3)}(\bar{m}_{q,k}^2)] \right\}. \end{aligned} \quad (25)$$

with the threshold function

$$\mathcal{BB}_{(2,2)}(\bar{m}_{\pi,k}^2, \bar{m}_{\sigma,k}^2) = \frac{T}{k} \sum_{p_0} G_{\pi\pi}^2(p) G_{\sigma\sigma}^2(p), \quad (26)$$

and $\mathcal{F}_{(n)}$ given in Eq. (31). The explicit analytic expressions are given in [1, 30]. In (25), the effective action is expanded about $\bar{\rho} = \bar{\kappa}_k$ with $\bar{\kappa}_k = Z_{\phi,k}\kappa$. In contrast to the standard expansion about the flowing minimum, we use a Taylor expansion about a fixed $\rho = \kappa$ with $\partial_t \kappa = 0$, as put forward in [30]. Hence, $\partial_t \bar{\kappa}_k = -\eta_{\phi,k} \bar{\kappa}_k$.

Note that the quark anomalous dimension $\eta_{q,k}(p_0)$ is in general complex-valued at finite chemical potential. As discussed in the previous section, this is related to the fact that correlation functions that involve quarks are functions of $p_0 + i\mu$, which again is related to the Silver Blaze property. Also, inserting $\eta_{q,k}(p_0)$ in (24) into the flows of other couplings or the effective potential leads to two-loop frequency resummations that properly take into account the non-regularised frequency dependence of the flows.

As already discussed above, for the Yukawa coupling $\bar{h}_k(p)$ we follow the procedure in [1]: We evaluate the coupling at a fixed external frequency $\text{Im } p_0 + i\mu = 0$, and $\vec{p} = 0$. The real part of p_0 is fixed by the requirement that h_k has to be temperature-independent at energy scales that exceed the thermal scale, i.e. $k \gtrsim \pi T$ and

depends only on the lowest Matsubara mode for $k \lesssim \pi T$. This suggest $p_0^2 = k^2 + (\pi T)^2 \Theta_T(k/T)$. The comprehensible choice $\Theta_T(x) = \exp(-2x/5)$ distinguishes between the low- and high-energy regime relative to the thermal scale. This can be viewed as a phenomenologically motivated procedure to circumvent the necessity of a fully frequency dependent Yukawa coupling \bar{h}_k . The flow of \bar{h}_k also depends on the frequency-dependent anomalous dimension $\eta_{q,k}(q_0)$ with the loop frequency q_0 , leading to two-loop contributions in the flow of the Yukawa coupling. In the context of the present work the latter is only relevant for the flow of the effective potential, where the frequency resummations in the flow of the Yukawa coupling relate to three-loop frequency effects which we consider to be sub-leading. We therefore drop the frequency dependence of $\eta_{q,k}$ in the flow of \bar{h}_k and use the same approximation as for the frequency dependence of $\partial_t \bar{h}_k$ also for the quark anomalous dimension in the diagram. This leads us to the same flow for \bar{h}_k as used in [1],

$$\begin{aligned} \partial_t \bar{h}_k &= \left(\frac{1}{2} \eta_{\phi,k} + \eta_{q,k} \right) \bar{h}_k + \frac{1}{4\pi^2 N_f} \bar{h}_k^3 \\ &\times \left[L_{(1,1)}^{(4)} (\bar{m}_{q,k}^2, \bar{m}_{\sigma,k}^2, \eta_{q,k}, \eta_{\phi,k}; p_0) \right. \\ &\left. - (N_f^2 - 1) L_{(1,1)}^{(4)} (\bar{m}_{q,k}^2, \bar{m}_{\pi,k}^2, \eta_{q,k}, \eta_{\phi,k}; p_0) \right], \end{aligned} \quad (27)$$

with

$$L_{(1,1)}^{(4)} = \frac{2}{3} \left[\left(1 - \frac{\eta_{\phi,k}}{5} \right) \mathcal{FB}_{(1,2)} + \left(1 - \frac{\eta_{q,k}}{4} \right) \mathcal{FB}_{(2,1)} \right]. \quad (28)$$

We omitted the arguments for the sake of brevity here. They are the same as in (24) and are defined in App. A. Note that the full Yukawa coupling $h_k(p_0) = Z_{q,k}(p_0) \bar{h}_k$ carries the relevant frequency dependence.

Finally, we discuss the flow equation of the effective potential. This is now derived in the presence of the frequency dependence of $Z_{q,k}(p_0)$. To illustrate this procedure, we first take a closer look at the structure of this equation. One can rewrite the flow of the quark contribution, $\partial_t V_k^q$ to the effective potential (up to a volume factor) as

$$\begin{aligned} \partial_t V_k^q &= -\text{tr } T \sum_{q_0} \int_{\vec{q}} G_{\bar{q}q}(q_0, \vec{q}) \partial_t R_k^q(q_0, \vec{q}) \\ &= -\text{tr } T \sum_{q_0} \int_{\vec{q}} G_{\bar{q}q}(q_0, \vec{q}) \vec{\gamma} \vec{q} (\partial_t - \eta_{q,k}(q_0)) r_F(\vec{q}) \\ &= \partial_t V_k^q \Big|_{\eta_{q,k}=0} + \Delta \partial_t V_k^q, \end{aligned} \quad (29)$$

where the trace sums over color, flavor and spinor indices. In the last line of (29) we have split the flow into a contribution with and without the quark anomalous dimension. The frequency summations carry a two-loop

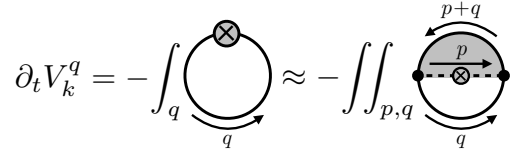


FIG. 2. Simplified illustration of the quark loop contribution to the flow of the effective potential. The first loop represents the standard form of the quark contribution. The crossed circle is the regulator insertion and the loop momentum integral also includes the frequency summation. The last term corresponds to $\Delta \partial_t V_k^q$ in Eq. (29). It illustrates how the full frequency dependence of the quark anomalous dimension enters here. The gray area corresponds to the contribution from the quark anomalous dimension. We dropped $\partial_t V_k^q \Big|_{\eta_{q,k}=0}$ in the last term for the sake of simplicity.

structure due to the frequency-dependent quark anomalous dimension $\eta_{q,k}(p_0)$. The quark propagator that enters in $\eta_{q,k}$ carries both frequencies via $q_0 + p_0$. This is illustrated in Fig. 2. In addition, the color trace has to be performed after the frequency summation in the presence of a non-vanishing temporal gluon background. This will be discussed at the end of this section.

The two-loop summation can be carried out analytically and we still arrive at an analytic expression for the flow equation of the effective potential,

$$\begin{aligned} \partial_t V_k(\rho) &= \frac{k^4}{360\pi^2} \left\{ 12(5 - \eta_{\phi,k}) [(N_f^2 - 1) \mathcal{B}_{(1)}(\bar{m}_{\pi,k}^2) \right. \\ &\quad + \mathcal{B}_{(1)}(\bar{m}_{\sigma,k}^2)] - 5N_c \left(48N_f \mathcal{F}_{(1)}(\bar{m}_{F,k}^2) \right. \\ &\quad + \frac{1}{2\pi^2} (-4 + \eta_{\phi,k}) \bar{h}_k^2 \left[\mathcal{FFB}_{(1,1,2)}(\bar{m}_{F,k}^2, \bar{m}_{\sigma,k}^2) \right. \\ &\quad \left. \left. + (N_f^2 - 1) \mathcal{FFB}_{(1,1,2)}(\bar{m}_{F,k}^2, \bar{m}_{\pi,k}^2) \right] \right\}, \end{aligned} \quad (30)$$

with the threshold functions, see also [1]

$$\mathcal{B}_{(n)} = \frac{T}{k} \sum_{p_0} G_{\phi\phi}^n(p) \quad \text{and} \quad \mathcal{F}_{(n)} = \frac{T}{k} \sum_{p_0} G_{\bar{q}q}^n(p). \quad (31)$$

The new contributions from the frequency dependent quark anomalous dimension are the last two lines of (30) with the new threshold functions $\mathcal{FFB}_{(1,1,2)}$. They encode the two-loop frequency summation discussed above and read schematically

$$\mathcal{FFB}_{(1,1,2)} = \frac{T^2}{k^2} \sum_{p_0} \sum_{q_0} G_{\bar{q}q}(q) G_{\bar{q}q}(p+q) G_{\phi\phi}^2(p). \quad (32)$$

This summation can be performed analytically and the result is given in App. A.

It is remarkable that, although $\eta_{q,k}(p_0)$ is complex-valued at finite μ , the flow equation (30) itself is manifestly real-valued when the frequency dependence is

taken into account. This is in accordance with our previous discussion: real-valued physical observables that respect the Silver Blaze property have to comprise the frequency dependence of the corresponding baryon number carrying correlation functions.

Finally, we evaluate the color trace which is crucial for the correct implementation of the Polyakov loop dynamics. The coupling between the gauge and the matter sector is achieved by considering a non-vanishing temporal gluon background field A_0 . In practice, this amounts to an imaginary shift of the chemical potential in the equations for the matter sector, $\mu \rightarrow \mu + igA_0$. Hence, one can carry out the Matsubara summation in Eq. (30) without any reference to the presence of gluons and simply shift the chemical potential after the summation. However, since $A_0 = A_0^a t^a$ with $t^a \in SU(3)$ is in the adjoint representation, the color trace has to be performed after the shift. Even though A_0 can always be rotated into the Cartan subalgebra of the gauge group, the color trace is rather involved in this case due to the two-loop frequency summation. However, it is always possible to re-express the A_0 -dependence in favor of the Polyakov loops L, \bar{L} since the chemical potential enters the flow equation through Fermi distribution functions n_F . The analytical result of this procedure can be found in App. A. Since the glue sector only couples to the quarks, only the threshold function $\mathcal{F}\mathcal{B}_{(1,1,2)}$ is involved.

IV. NUMERICAL RESULTS

In the last chapter we have derived the flow equation of the effective potential of the low-energy effective theory, (30) with (27) and the quark and meson anomalous dimensions (24) and (25). It is left to specify the initial effective action and the UV-cutoff of the effective theory.

The latter is chosen $\Lambda = 700 \text{ MeV}$ in order to keep as many matter fluctuations as possible while maximising the glue decoupling on the other hand. See [1] for more details. At this initial UV scale we approximate the initial effective potential by

$$\bar{V}_\Lambda(\bar{\rho}) = \frac{\bar{\lambda}_\Lambda}{2} \bar{\rho}^2 + \bar{\nu}_\Lambda \bar{\rho}. \quad (33)$$

In addition to the two couplings $\bar{\lambda}_\Lambda$ and $\bar{\nu}_\Lambda$ the Yukawa coupling \bar{h}_Λ and the explicit chiral symmetry breaking parameter \bar{c}_Λ have to be provided.

Truncations	$\bar{\lambda}_\Lambda$	$\bar{\nu}_\Lambda [\text{GeV}^2]$	\bar{h}_Λ	$\bar{c}_\Lambda [\times 10^{-3} \text{GeV}^3]$
with frequency dependence	20.7	0.24	7.2	1.96
without	9.7	0.31	7.2	1.96

TABLE II. Input parameters for the truncation with and without frequency-dependent quark anomalous dimension, cf. Eq. (30).

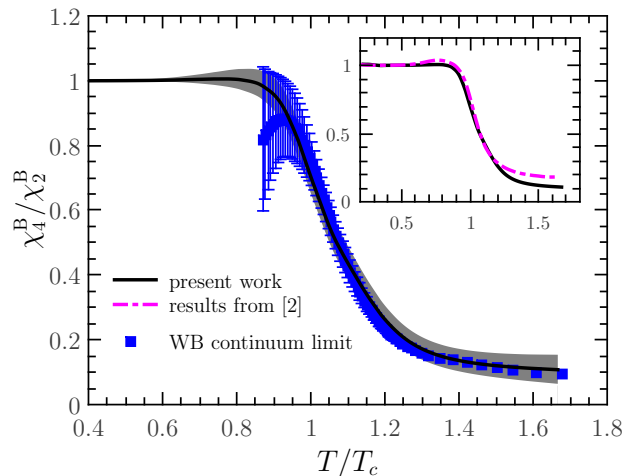


FIG. 3. Kurtosis $\kappa\sigma^2 = \chi_4^B / \chi_2^B$ of the baryon number distribution in comparison with continuum-extrapolated lattice results from the Wuppertal-Budapest collaboration [16]. The gray band shows an error estimate according to Eq. (34). The inlay shows a comparison between our present result for the kurtosis and the result of [2], where neither the frequency dependence, nor the Polyakov loop fluctuations have been taken into account.

These initial couplings are determined by fitting the pion decay constant $f_\pi = 92.5 \text{ MeV}$, the pion mass $m_\pi = 135 \text{ MeV}$, the σ -meson curvature mass $m_\sigma = 450 \text{ MeV}$, and the quark mass $m_q = 297 \text{ MeV}$ in the vacuum.

These observables do not fix the set of initial parameters completely. This allows us to imprint further QCD information in the model: as has been discussed in [2], the vacuum QCD flows of the couplings present in the effective theory are known from [32, 33]. Hence we utilise the remaining freedom in the set of initial parameters in order to imprint the known QCD-flow in the large cut-off regime of the effective theory for cutoff scales k close to Λ . Effectively this is done by simply minimising the meson fluctuations for large cutoff scales, as the mesons quickly decouple at these scales in full QCD. This leads to the upper parameter set in Tab. II. For an evaluation of the fluctuation physics carried by the frequency dependence we compare the full results with that obtained in the approximation used in [2], see lower parameter set in Tab. II. Note that in comparison to [2] we have also changed the Polyakov loop effective potential, for the discussion see chapter II A.

Fig. 3 summarises our results for the fluctuations at vanishing density as a function of temperature: we show the kurtosis of baryon number distributions, the ratio between the quartic and quadratic baryon number fluctuations, as a function of the temperature in comparison with the continuum-extrapolated lattice results from the Wuppertal-Budapest collaboration [16]. While our computation is done in a $N_f = 2$ flavor low energy effective theory, the lattice results are obtained for $N_f = 2 + 1$. Such a comparison necessitates the introduction of reduced or relative temperatures, and the absolute temper-

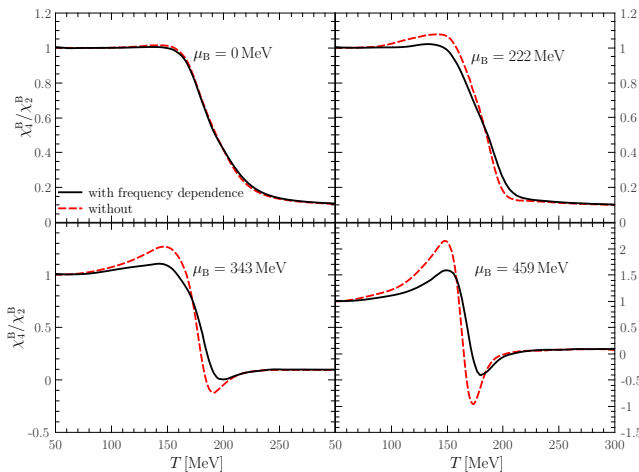


FIG. 4. Kurtosis as a function of the temperature for different baryon chemical potentials. Solid lines include the frequency dependence of the quark anomalous dimension and dashed lines not.

atures are rescaled by their corresponding pseudo-critical temperature T_c . We have chosen $T_c = 155$ MeV for the $2+1$ flavor lattice simulation, which is obtained from χ_4^B simulations in [53]. This number is also consistent with the calculations in [54]. For the $N_f = 2$ computations the pseudo-critical temperature is $T_c = 180$ MeV, which is related to the maximal magnitude of the derivative of $\bar{\rho}_{\text{EoM}}$, in the effective potential, with respect to the temperature.

The grey band in Fig. 3 gives a rough estimate of the systematic error for the computation. It relates to the temperature dependence of the initial condition of the effective action, and can be estimated by that of the flow at $k = \Lambda$, for more details see [1, 29]. This leads to the estimate

$$\frac{\chi_4^B}{\chi_2^B} \pm \Delta \frac{\chi_4^B}{\chi_2^B} = \frac{\chi_4^B}{\chi_2^B} \left(1 \pm \frac{4}{e^{\Lambda/T} - 1} \right), \quad (34)$$

with $\Lambda = 700$ MeV. We find that both the kurtosis calculated with the frequency dependence and that without, see also Fig. 4, agree with the lattice results over the full temperature range. While the effect of the frequency dependence is only minor at vanishing density, the Polyakov loop potential we use in the present work is of major importance at large temperatures. This is due to the fact that, in contrast to the potential used in [1, 2], this potential also correctly captures the effect of Polyakov loop fluctuations above T_c , see [36]. It is precisely this regime where the present results at vanishing density differ from that in [2], see the inlay figure in Fig. 3. Moreover, the

\sqrt{s} [GeV]	200	62.4	39	27	19.6	11.5	7.7
$\mu_{B,N_f=2}$ [MeV]	25.3	78.1	121	168.7	222.7	343	459.4

TABLE III. $\mu_{B,N_f=2}$ corresponding to different collision energy, with Eq. (35), for details see [2].

current results agree quantitatively with the lattice results. This emphasises the importance of Polyakov loop fluctuations for the baryon number fluctuations or more generally higher order correlations as discussed in [1].

In Fig. 4 we compare the dependence of kurtosis on the temperature at several values of the baryon chemical potential for the two cases with and without the frequency dependence. Here $\mu_B = 0, 222, 343, 459$ MeV are chosen. We have found that the difference of the kurtosis irrespective of the frequency dependence is small at vanishing baryon chemical potential. However, we argued in Sec. III that the frequency is intimately related to the chemical potential dependence and therefore expect that this will increasingly important with increasing μ . Indeed, we find that the frequency dependence improved effective potential has a large effect on the kurtosis at large μ . The frequency dependence reduces the amplitude of the kurtosis significantly during the crossover. Our finding implies that the frequency dependence of the quark anomalous dimension is important and indispensable for STAR, CBM and HADES-related physics.

Similarly to [2] we can map our results of the skewness and kurtosis as functions of temperature and chemical potential in $N_f = 2$ flavor QCD to that of the kurtosis at freeze-out temperatures as a function of the collision energy \sqrt{s} in $N_f = 2+1$ flavor QCD. This is done by an appropriate rescaling of the dimensionful quantities that captures the different scale-dependence in both theories. Firstly we adopt the same relation between the chemical potentials in these theories as [2], which is derived from the experimentally measured skewness $S\sigma = \chi_3^B/\chi_2^B$ and the $\sigma^2/M = \chi_2^B/\chi_1^B$ in [6]. This leads to

$$\mu_{B,N_f=2} \approx 1.13 \mu_{B,N_f=2+1}, \quad (35)$$

The respective collision energies are summarised in Tab. III. In this table all collisions energies are far away from the critical endpoint of the model.

We use the same systematic error estimate as in [2], accounting for the uncertainties in determining the freeze-out temperature, the chemical potential as well as the collision energy in the present set-up.

This leads us to Fig. 5, the comparison to the results in [2] is shown in the inlay. Both results agree within the respective systematic error bands for collision energies $\sqrt{s} \gtrsim 19$ GeV. This is the region which has been singled out by an evaluation of the systematic error in [2] as the trustworthy one, and our current results confirm non-trivially this analysis. For smaller collision energies $\sqrt{s} \lesssim 19$ GeV the systematic errors dominate the result, in Fig. 5 the error band only shows the error arising from the inaccurate determination of the different temperature and chemical potential scales.

However, it is the qualitative improvement of the current set-up in comparison to [2], that already allows for interesting conclusions: while in the earlier work the experimental results were compatible with the computation also for $\sqrt{s} \lesssim 19$ GeV due to the large error bands, the current findings clearly deviate at these collision ener-

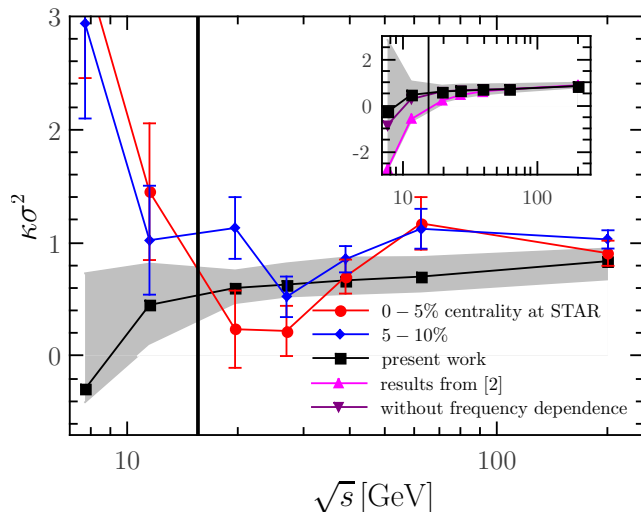


FIG. 5. Calculated kurtosis $\kappa\sigma^2$ as a function of the collision energy, in comparison with experimental measurements in Au+Au collisions at RHIC with centralities 0–5%, 5–10% [6]. Following [2], we show error estimates resulting from the determination of freeze-out temperatures with the gray region, and on the left hand side of the black vertical line, the UV-cutoff effect becomes significant.

gies. Possible important sources of the incompatibilities in this regime are, on the one hand, omitted effects, such as the missing high density off-shell degrees of freedom in our present computations. Potentially, they have a significant impact on the existence and location of a possible critical endpoint, as well as on the size of the critical region. Furthermore, the lack of non-equilibrium effects, see e.g. [55], has to be remedied. On the other hand, the centrality dependence, or, more accurately, the dependence on the p_T -cut of the experimental results has to be taken into account, see e.g. [56, 57]. Generally speaking, there are further non-critical sources of fluctuations that affect the measured baryon number multiplicity distributions and are not completely accounted for in the data. For a recent summary of these issues we refer to [58] and references therein. The discussion of these effects is deferred to future work.

V. SUMMARY AND CONCLUSIONS

In this work we have studied the QCD thermodynamics, the baryon number fluctuations, and the kurtosis of the baryon number distributions in a low-energy effective model with fluctuations. Quantum, thermal, and density fluctuations are included within the framework of the functional renormalisation group, see [1, 2]. In comparison to these previous calculations, qualitative improvements have been included here. Firstly, we have considered the effects of a non-trivial quark-dispersion via the inclusion of the frequency dependence of the quark anomalous dimension. The frequency dependence has

been considered on the level of an analytic resummation in terms of a cutoff-dependent two-loop Matsubara sum. Secondly, we have used a Polyakov loop potential that takes care of the second order correlations of the Polyakov loop, see [36].

These qualitative improvements reduce significantly the systematic error of the current set-up in particular in the regime relevant for STAR, CBM and HADES measurements. On the more technical side, the frequency dependence considered here implements naturally the Silver Blaze property of the theory: at vanishing temperature all correlation functions show no explicit μ -dependence, the only μ -dependence is that of the frequency arguments for modes with non-vanishing baryon number, i.e. $p_0 + i\mu$ for quarks. We believe, that the technical set-up put forward in the present work takes into account the relevant frequency effects on a semi-quantitative level.

The baryon number fluctuations obtained with frequency dependence are compared with those without the dependence. This inevitably also includes non-trivial interactions between quarks and gluons at higher order, that have been derived here for the first time. We find the difference between them is mild at vanishing baryon chemical potential, but increases with the chemical potential, which implies that the frequency dependence of the quark anomalous dimension plays an important role in CEP-related physics. Furthermore, our calculated kurtosis of the baryon number distribution is compared with the lattice results. Our results are in very good agreement with the lattice simulations over the full temperature range available.

The above improvements allowed for an update of the comparison of (equilibrium) kurtosis as a function of the collision energy with the STAR data, see Fig. 5. In comparison to the previous works the qualitatively reduced error band allows for a more conclusive analysis in particular at low collision energies (high density), for the detailed discussion see the discussion below Eq. (35): the situations hints strongly towards missing effects of the p_T -cuts as well as that of non-equilibrium fluctuations, as well as suggesting a direct study in $N_f = 2 + 1$ flavor QCD. The latter extension is work in progress, and we also plan to extend the current work towards non-equilibrium effects as well as an analysis of the p_T -cut.

ACKNOWLEDGMENTS

We thank M. Mitter and Nils Strodthoff for discussions and work on related subjects. This work is supported by the AvH foundation, EMMI, the BMBF grants 05P12VHCTG and 05P15VHFC1, the grant ERC-AdG-290623, the FWF grant P24780-N27, HIC for FAIR, and the DFG via SFB 1225 (ISOQUANT).

Appendix A: Threshold functions

The mixed fermion-boson threshold functions at finite temperature T and chemical potential μ are in general defined by a product of i fermion propagators

$$G_F(q, \bar{m}_{F,k}^2) = \frac{1}{(\tilde{q}_0 + i\tilde{\mu})^2 + 1 + \bar{m}_{F,k}^2}, \quad (\text{A1})$$

and j boson propagators

$$G_B(q, \bar{m}_{B,k}^2) = \frac{1}{\tilde{q}_0^2 + 1 + \bar{m}_{B,k}^2}, \quad (\text{A2})$$

with the dimensionless $\tilde{\mu} = \mu/k$, $\tilde{q}_0 = q_0/k$ and momenta $q_0 = (2n+1)\pi T$ for fermions and $q_0 = 2n\pi T$ for bosons ($n \in \mathbb{Z}$), as

$$\mathcal{FB}_{(i,j)}(\bar{m}_{F,k}^2, \bar{m}_{B,k}^2; p_0) \equiv \frac{T}{k} \sum_n G_F^i(q, \bar{m}_{F,k}^2) G_B^j(p - q, \bar{m}_{B,k}^2). \quad (\text{A3})$$

Note that with the $3d$ flat cutoffs used in the present work, the propagators only depend on the frequencies. For $(i, j) \neq (1, 1)$ these threshold functions can be generated by corresponding mass derivatives from $\mathcal{FB}_{(1,1)}$ as follows

$$\mathcal{FB}_{(i,j)}(\bar{m}_{F,k}^2, \bar{m}_{B,k}^2; p_0) = \frac{(-1)^{i+j-2}}{(i-1)!(j-1)!} \frac{\partial^{i-1}}{\partial \bar{m}_{F,k}^{2(i-1)}} \frac{\partial^{j-1}}{\partial \bar{m}_{B,k}^{2(j-1)}} \mathcal{FB}_{(1,1)}(\bar{m}_{F,k}^2, \bar{m}_{B,k}^2; p_0). \quad (\text{A4})$$

The Matsubara sum in the first threshold function $\mathcal{FB}_{(1,1)}$ can be evaluated analytically

$$\mathcal{FB}_{(1,1)}(\bar{m}_{F,k}^2, \bar{m}_{B,k}^2; p_0) = \frac{k^3}{2} \left\{ - \frac{n_B(\bar{m}_{B,k}^2; T)}{E_B \left[(ip_0 - \mu + E_B)^2 - E_F^2 \right]} - \frac{n_B(\bar{m}_{B,k}^2; T) + 1}{E_B \left[(ip_0 - \mu - E_B)^2 - E_F^2 \right]} + \frac{\bar{n}_F(\bar{m}_{F,k}^2; T, \mu)}{E_F \left[(ip_0 - \mu - E_F)^2 - E_B^2 \right]} + \frac{n_F(\bar{m}_{F,k}^2; T, \mu) - 1}{E_F \left[(ip_0 - \mu + E_F)^2 - E_B^2 \right]} \right\}. \quad (\text{A5})$$

In this expression the quasi-particle energies

$$E_i = k\sqrt{1 + \bar{m}_{i,k}^2}, \quad i = F, B, \quad (\text{A6})$$

appear with the corresponding distribution functions

$$n_B(\bar{m}_{B,k}^2; T) = \frac{1}{e^{E_B/T} - 1},$$

$$n_F(\bar{m}_{F,k}^2; T, \mu) = \frac{1}{e^{(E_F - \mu)/T} + 1},$$

$$\bar{n}_F(\bar{m}_{F,k}^2; T, \mu) = n_F(\bar{m}_{F,k}^2; T, -\mu), \quad (\text{A7})$$

In the same way, the threshold function consisting of one boson and two fermion propagators with different frequencies are defined as

$$\mathcal{F}\mathcal{FB}_{(i,j,k)}(\bar{m}_{F,k}^2, \bar{m}_{B,k}^2) \equiv \frac{T^2}{k^2} \sum_{n_p} \sum_{n_q} G_F^i(p, \bar{m}_{F,k}^2) G_F^j(q, \bar{m}_{F,k}^2) G_B^k(p - q, \bar{m}_{B,k}^2). \quad (\text{A8})$$

Note that there are two separate Matsubara summations involved, which are indispensable to recover the correct μ -dependency. We have chosen a slightly different momentum routing here as compared to Fig. 2 and Eq. (32). The result is, of course, independent of this choice of the routing as long as momentum conservation is maintained.

Similar to (A4) higher threshold functions with $(i, j, k) \neq (1, 1, 1)$ can be generated by corresponding mass derivatives from $\mathcal{F}\mathcal{FB}_{(1,1,1)}$ like

$$\mathcal{F}\mathcal{FB}_{(1,1,2)}(\bar{m}_{F,k}^2, \bar{m}_{B,k}^2) = - \frac{\partial}{\partial \bar{m}_{B,k}^2} \mathcal{F}\mathcal{FB}_{(1,1,1)}(\bar{m}_{F,k}^2, \bar{m}_{B,k}^2), \quad (\text{A9})$$

which is needed in Eq. (30).

The first threshold function $\mathcal{F}\mathcal{FB}_{(1,1,1)}$ can again be performed analytically with the result

$$\mathcal{F}\mathcal{FB}_{(1,1,1)}(\bar{m}_{F,k}^2, \bar{m}_{B,k}^2) = f_{cp1} \left[(1 - \bar{n}_F) \bar{n}_{(F+B)} + (1 - n_F) (-2 + n_{(F+B)}) + n_B (-2 + \bar{n}_F + \bar{n}_{(F+B)} + n_F + n_{(F+B)}) \right] + f_{cp2} \left[\bar{n}_F^2 + (1 - n_F)^2 \right] + \left\{ f_{cn1} \left[-\bar{n}_F (1 + \bar{n}_{(F-B)}) - n_F (-1 + n_{(F-B)}) - n_B (-2 + \bar{n}_F + \bar{n}_{(F-B)} + n_F + n_{(F-B)}) \right] + f_{cn2} \bar{n}_F (1 - n_F) \right\} / (3 - \bar{m}_{B,k}^2 + 4\bar{m}_{F,k}^2), \quad (\text{A10})$$

Note that besides the standard distribution functions n_B , n_F , \bar{n}_F , Eqs. (A7), several new functions, which incorporate the nontrivial μ -dependence, emerge in $\mathcal{F}\mathcal{FB}_{(1,1,1)}$.

These new distribution functions are given explicitly by

$$n_{(F\pm B)} = \frac{1}{e^{(E_F \pm E_B - \mu)/T} + 1} . \quad (\text{A11})$$

The other \bar{n} combinations are obtained by the corresponding n functions with the replacement $\mu \rightarrow -\mu$. In (A10), the coefficients are defined by

$$\begin{aligned} f_{cp1} &= \frac{k^4}{4E_B E_F (E_B^2 + 2E_B E_F)}, \\ f_{cp2} &= \frac{k^4}{4E_B^2 E_F^2}, \\ f_{cn1} &= \frac{k^2(E_B + 2E_F)}{4E_B^2 E_F}, \\ f_{cn2} &= \frac{k^2}{2E_F^2}. \end{aligned} \quad (\text{A12})$$

It is left to specify the relevant threshold functions, when the coupling between the gluonic background fields and the quarks is taken into account. In this case, $\mathcal{FFB}_{(1,1,1)}$ in (A10) takes the following modified form:

$$\begin{aligned} \mathcal{FFB}_{(1,1,1)}(\bar{m}_{F,k}^2, \bar{m}_{B,k}^2) \Big|_{\text{modified}} = & \\ f_{cp1} \Big[-\bar{n}_{F,(F+B)} - n_{F,(F+B)} + n_F + \bar{n}_{(F+B)} - 1 & \\ + n_B(-2 + \bar{n}_F + \bar{n}_{(F+B)} + n_F + n_{(F+B)}) \Big] & \\ + f_{cp2}(\bar{n}_{F,F} + n_{F,F}) + \left\{ -f_{cn1} \Big[n_{F,(F-B)} + \bar{n}_{F,(F-B)} & \right. \\ + \bar{n}_F + n_{(F-B)} - 1 + n_B(-2 + \bar{n}_F + \bar{n}_{(F-B)} & \\ + n_F + n_{(F-B)}) \Big] + f_{cn2} n'_{F,F} \Big\} & \\ \Big/ (3 - \bar{m}_{B,k}^2 + 4\bar{m}_{F,k}^2). & \end{aligned} \quad (\text{A13})$$

In comparison with (A10) there are several new distribu-

tion functions, whose explicit expressions are given by

$$\begin{aligned} n_{F,(F\pm B)} &= \frac{1}{2} \left[4n_{2F} n_{2(F\pm B)} (L^2 - \bar{L}) + n_{1F} n_{1(F\pm B)} \right. \\ &\quad \times (\bar{L}^2 - L) + (L\bar{L} - 1)(n_{1F} n_{2(F\pm B)} \\ &\quad \left. + n_{2F} n_{1(F\pm B)}) + 2(n_F - 1)(n_{(F\pm B)} - 1) \right], \end{aligned} \quad (\text{A14})$$

and

$$\begin{aligned} \bar{n}_{F,(F\pm B)} &= \frac{1}{2} \left[4\bar{n}_{2F} \bar{n}_{2(F\pm B)} (\bar{L}^2 - L) + \bar{n}_{1F} \bar{n}_{1(F\pm B)} \right. \\ &\quad \times (L^2 - \bar{L}) + (L\bar{L} - 1)(\bar{n}_{1F} \bar{n}_{2(F\pm B)} \\ &\quad \left. + \bar{n}_{2F} \bar{n}_{1(F\pm B)}) + 2\bar{n}_F \bar{n}_{(F\pm B)} \right], \end{aligned} \quad (\text{A15})$$

$$\begin{aligned} n_{F,F} &= 2n_{2F}^2 (L^2 - \bar{L}) + \frac{1}{2}n_{1F}^2 (\bar{L}^2 - L) \\ &\quad + n_{1F} n_{2F} (L\bar{L} - 1) + (n_F - 1)^2, \end{aligned} \quad (\text{A16})$$

$$\begin{aligned} n'_{F,F} &= \bar{n}_{1F} n_{2F} (L^2 - \bar{L}) + n_{1F} \bar{n}_{2F} (\bar{L}^2 - L) \\ &\quad + \frac{1}{4}(L\bar{L} - 1)(\bar{n}_{1F} n_{1F} + 4\bar{n}_{2F} n_{2F}) \\ &\quad - \bar{n}_F (n_F - 1), \end{aligned} \quad (\text{A17})$$

$$\begin{aligned} \bar{n}_{F,F} &= 2\bar{n}_{2F}^2 (\bar{L}^2 - L) + \frac{1}{2}\bar{n}_{1F}^2 (L^2 - \bar{L}) \\ &\quad + \bar{n}_{1F} \bar{n}_{2F} (L\bar{L} - 1) + \bar{n}_F^2, \end{aligned} \quad (\text{A18})$$

where we have defined

$$\begin{aligned} n_{1F}(x, T, L, \bar{L}) &= \frac{2e^{x/T}}{\left(1 + 3\bar{L}e^{x/T} + 3Le^{2x/T} + e^{3x/T}\right)}, \\ n_{2F}(x, T, L, \bar{L}) &= \frac{e^{x/T}}{2} n_{1F}(x, T, L, \bar{L}), \end{aligned} \quad (\text{A19})$$

with $i = 1, 2$

$$\begin{aligned} n_{iF} &= n_{iF}(E_F - \mu, T, L, \bar{L}), \\ n_{i(F\pm B)} &= n_{iF}(E_F \pm E_B - \mu, T, L, \bar{L}). \end{aligned} \quad (\text{A20})$$

The other \bar{n} functions are obtained by replacing $\mu \rightarrow -\mu$, $\bar{L} \rightarrow L$ and $L \rightarrow \bar{L}$.

[1] W.-j. Fu and J. M. Pawłowski, Phys. Rev. **D92**, 116006 (2015), arXiv:1508.06504 [hep-ph].

[2] W.-j. Fu and J. M. Pawłowski, Phys. Rev. **D93**, 091501

- (2016), arXiv:1512.08461 [hep-ph].
- [3] M. Stephanov, PoS **LAT2006**, 024 (2006), arXiv:hep-lat/0701002 [hep-lat].
 - [4] L. Adamczyk *et al.* (STAR), Phys.Rev.Lett. **112**, 032302 (2014), arXiv:1309.5681 [nucl-ex].
 - [5] L. Adamczyk *et al.* (STAR), Phys. Rev. Lett. **113**, 092301 (2014), arXiv:1402.1558 [nucl-ex].
 - [6] X. Luo (STAR), *9th International Workshop on Critical Point and Onset of Deconfinement (CPOD 2014) Bielefeld, Germany, November 17-21, 2014*, PoS **CPOD2014**, 019 (2014), arXiv:1503.02558 [nucl-ex].
 - [7] S. Chattopadhyay *et al.* (for the CBM), (2016), arXiv:1607.01487 [nucl-ex].
 - [8] G. Aarts (2015) arXiv:1512.05145 [hep-lat].
 - [9] J. M. Pawłowski, Nucl.Phys. **A931**, 113 (2014).
 - [10] M. A. Stephanov, K. Rajagopal, and E. V. Shuryak, Phys.Rev.Lett. **81**, 4816 (1998), arXiv:hep-ph/9806219 [hep-ph].
 - [11] M. A. Stephanov, K. Rajagopal, and E. V. Shuryak, Phys. Rev. **D60**, 114028 (1999), arXiv:hep-ph/9903292 [hep-ph].
 - [12] M. A. Stephanov, Phys. Rev. Lett. **102**, 032301 (2009), arXiv:0809.3450 [hep-ph].
 - [13] B. Berdnikov and K. Rajagopal, Phys. Rev. **D61**, 105017 (2000), arXiv:hep-ph/9912274 [hep-ph].
 - [14] S. Mukherjee, R. Venugopalan, and Y. Yin, Phys. Rev. **C92**, 034912 (2015), arXiv:1506.00645 [hep-ph].
 - [15] S. Mukherjee, R. Venugopalan, and Y. Yin, (2016), arXiv:1605.09341 [hep-ph].
 - [16] S. Borsanyi, Z. Fodor, S. Katz, S. Krieg, C. Ratti, *et al.*, Phys.Rev.Lett. **111**, 062005 (2013), arXiv:1305.5161 [hep-lat].
 - [17] H.-T. Ding, *Proceedings, 24th International Conference on Ultra-Relativistic Nucleus-Nucleus Collisions (Quark Matter 2014)*, Nucl. Phys. **A931**, 52 (2014), arXiv:1408.5236 [hep-lat].
 - [18] V. Skokov, B. Stokic, B. Friman, and K. Redlich, Phys.Rev. **C82**, 015206 (2010), arXiv:1004.2665 [hep-ph].
 - [19] V. Skokov, B. Friman, E. Nakano, K. Redlich, and B.-J. Schaefer, Phys.Rev. **D82**, 034029 (2010), arXiv:1005.3166 [hep-ph].
 - [20] V. Skokov, B. Friman, and K. Redlich, Phys.Rev. **C83**, 054904 (2011), arXiv:1008.4570 [hep-ph].
 - [21] F. Karsch, B.-J. Schaefer, M. Wagner, and J. Wambach, Phys.Lett. **B698**, 256 (2011), arXiv:1009.5211 [hep-ph].
 - [22] W.-j. Fu, Y.-x. Liu, and Y.-L. Wu, Phys.Rev. **D81**, 014028 (2010), arXiv:0910.5783 [hep-ph].
 - [23] W.-j. Fu and Y.-L. Wu, Phys. Rev. **D82**, 074013 (2010), arXiv:1008.3684 [hep-ph].
 - [24] B. J. Schaefer and M. Wagner, Phys. Rev. **D85**, 034027 (2012), arXiv:1111.6871 [hep-ph].
 - [25] B.-J. Schaefer and M. Wagner, Central Eur.J.Phys. **10**, 1326 (2012), arXiv:1203.1883 [hep-ph].
 - [26] K. Morita, B. Friman, and K. Redlich, Phys. Lett. **B741**, 178 (2015), arXiv:1402.5982 [hep-ph].
 - [27] K. Morita and K. Redlich, PTEP **2015**, 043D03 (2015), arXiv:1409.8001 [hep-ph].
 - [28] L. M. Haas, R. Stiele, J. Braun, J. M. Pawłowski, and J. Schaffner-Bielich, Phys.Rev. **D87**, 076004 (2013), arXiv:1302.1993 [hep-ph].
 - [29] T. K. Herbst, M. Mitter, J. M. Pawłowski, B.-J. Schaefer, and R. Stiele, Phys.Lett. **B731**, 248 (2014), arXiv:1308.3621 [hep-ph].
 - [30] J. M. Pawłowski and F. Rennecke, Phys. Rev. D **90**, 076002 (2014), arXiv:1403.1179 [hep-ph].
 - [31] A. J. Helmboldt, J. M. Pawłowski, and N. Strodthoff, Phys.Rev. **D91**, 054010 (2015), arXiv:1409.8414 [hep-ph].
 - [32] M. Mitter, J. M. Pawłowski, and N. Strodthoff, Phys.Rev. **D91**, 054035 (2015), arXiv:1411.7978 [hep-ph].
 - [33] J. Braun, L. Fister, J. M. Pawłowski, and F. Rennecke, (2014), arXiv:1412.1045 [hep-ph].
 - [34] T. D. Cohen, Phys.Rev.Lett. **91**, 222001 (2003), arXiv:hep-ph/0307089 [hep-ph].
 - [35] N. Khan, J. M. Pawłowski, F. Rennecke, and M. M. Scherer, (2015), arXiv:1512.03673 [hep-ph].
 - [36] P. M. Lo, B. Friman, O. Kaczmarek, K. Redlich, and C. Sasaki, Phys.Rev. **D88**, 074502 (2013), arXiv:1307.5958 [hep-lat].
 - [37] T. K. Herbst, J. M. Pawłowski, and B.-J. Schaefer, Phys.Lett. **B696**, 58 (2011), arXiv:1008.0081 [hep-ph].
 - [38] B.-J. Schaefer, J. M. Pawłowski, and J. Wambach, Phys.Rev. **D76**, 074023 (2007), arXiv:0704.3234 [hep-ph].
 - [39] K. Fukushima, Phys.Lett. **B591**, 277 (2004), arXiv:hep-ph/0310121 [hep-ph].
 - [40] C. Wetterich, Phys.Lett. **B301**, 90 (1993).
 - [41] H. Gies and C. Wetterich, Phys.Rev. **D65**, 065001 (2002), arXiv:hep-th/0107221 [hep-th].
 - [42] H. Gies and C. Wetterich, Phys.Rev. **D69**, 025001 (2004), arXiv:hep-th/0209183 [hep-th].
 - [43] J. M. Pawłowski, Annals Phys. **322**, 2831 (2007), arXiv:hep-th/0512261 [hep-th].
 - [44] S. Floerchinger and C. Wetterich, Phys.Lett. **B680**, 371 (2009), arXiv:0905.0915 [hep-th].
 - [45] C. Ratti, M. A. Thaler, and W. Weise, Phys.Rev. **D73**, 014019 (2006), arXiv:hep-ph/0506234 [hep-ph].
 - [46] W.-j. Fu, Z. Zhang, and Y.-x. Liu, Phys.Rev. **D77**, 014006 (2008), arXiv:0711.0154 [hep-ph].
 - [47] F. Rennecke, Phys. Rev. **D92**, 076012 (2015), arXiv:1504.03585 [hep-ph].
 - [48] A. K. Cyrol, L. Fister, M. Mitter, J. M. Pawłowski, and N. Strodthoff, (2016), arXiv:1605.01856 [hep-ph].
 - [49] T. K. Herbst, J. Luecker, and J. M. Pawłowski, (2015), arXiv:1510.03830 [hep-ph].
 - [50] J. Braun, L. M. Haas, F. Marhauser, and J. M. Pawłowski, Phys.Rev.Lett. **106**, 022002 (2011), arXiv:0908.0008 [hep-ph].
 - [51] K. Fukushima, Phys. Rev. **D77**, 114028 (2008), [Erratum: Phys. Rev.D78,039902(2008)], arXiv:0803.3318 [hep-ph].
 - [52] B.-J. Schaefer, M. Wagner, and J. Wambach, Phys.Rev. **D81**, 074013 (2010), arXiv:0910.5628 [hep-ph].
 - [53] R. Bellwied, S. Borsanyi, Z. Fodor, S. D. Katz, A. Pasztor, C. Ratti, and K. K. Szabo, (2015), arXiv:1507.04627 [hep-lat].
 - [54] S. Borsanyi *et al.* (Wuppertal-Budapest Collaboration), JHEP **1009**, 073 (2010), arXiv:1005.3508 [hep-lat].
 - [55] C. Herold, M. Nahrgang, Y. Yan, and C. Kobdaj, Phys. Rev. **C93**, 021902 (2016), arXiv:1601.04839 [hep-ph].
 - [56] A. Bzdak, R. Holzmann, and V. Koch, (2016), arXiv:1603.09057 [nucl-th].
 - [57] A. Bzdak, V. Koch, and N. Strodthoff, (2016), arXiv:1607.07375 [nucl-th].
 - [58] M. Nahrgang, in *25th International Conference on Ultra-Relativistic Nucleus-Nucleus Collisions (Quark Matter*

2015) Kobe, Japan, September 27-October 3, 2015 (2016)
arXiv:1601.07437 [nucl-th].